ACS APPLIED MATERIALS & INTERFACES

Research Article

www.acsami.org

Characterization of MoS_2–Graphene Composites for High-Performance Coin Cell Supercapacitors

Mark A. Bissett,*[,†] Ian A. Kinloch,[‡] and Robert A. W. Dryfe*[,†]

[†]School of Chemistry, University of Manchester, Oxford Road, Manchester M13 9PL, United Kingdom

[‡]School of Materials, University of Manchester, Oxford Road, Manchester M13 9PL, United Kingdom

Supporting Information

ABSTRACT: Two-dimensional materials, such as graphene and molybdenum disulfide (MoS_2), can greatly increase the performance of electrochemical energy storage devices because of the combination of high surface area and electrical conductivity. Here, we have investigated the performance of solution exfoliated MoS_2 thin flexible membranes as supercapacitor electrodes in a symmetrical coin cell arrangement using an aqueous electrolyte (Na_2SO_4). By adding highly conductive graphene to form nanocomposite membranes, it was possible to increase the specific capacitance by reducing the resistivity of the electrode and altering the morphology of the membrane. With continued charge/discharge cycles the performance of the membranes was found to increase significantly (up to 800%), because of partial re-exfoliation of the layered material with continued ion intercalation, as well as increasing the specific capacitance through intercalation pseudocapacitance. These results demonstrate a simple and scalable application of layered 2D materials toward electrochemical energy storage.

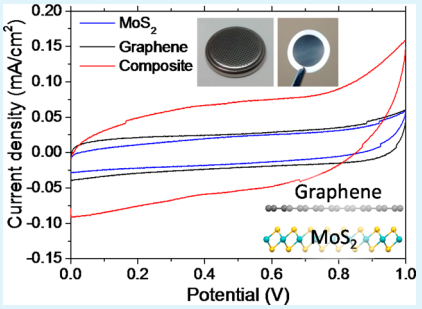

KEYWORDS: *graphene, MoS_2, supercapacitors, pseudocapacitors, electrochemistry, energy storage, coin cell*

INTRODUCTION

Two-dimensional (2D) materials such as graphene and molybdenum disulfide (MoS_2) are excellent candidates for applications in electrochemical energy storage because of their high available surface area and versatile electronic structure. Porous carbon materials, and graphene in particular, have been investigated previously for applications in electrochemical energy storage because of their many beneficial properties such as mechanical strength, high specific surface area (2675 m^2/g), and high thermal and electrical conductivity.[1−6] Other layered 2D materials such as transition metal dichalcogenides (TMDs) including MoS_2 have been investigated to a lesser extent but are gaining increased interest recently for integration into electronic devices due to similarities with graphene.[7,8] Exfoliated MoS_2 in particular possesses high catalytic activity which makes it an efficient hydrogen evolution catalyst[9−12] as well as a useful energy storage material for use in lithium and sodium ion batteries.[13,14] These layered 2D materials can be synthesized in several different ways including micromechanical peeling[15] and chemical vapor deposition,[15,16] but currently the most applicable for cost-effective, large scale production is through top down exfoliation of bulk powders via ultrasonic treatment in specially chosen solvents. This solution phase exfoliation has been demonstrated previously for graphene[17] and can be extended to other 2D materials[18,19] to create large volumes of monolayer and few layer flakes that can then be deposited onto a substrate or formed into films.

Supercapacitors are one application for which 2D materials can greatly increase performance and efficiency. Supercapacitors are unique because they provide a much higher power density than conventional batteries while also having a higher energy density than regular capacitors while still maintaining almost limitless cycling durability. With the continued miniaturization of electronic devices the need to create similarly miniature power sources is increasing, and supercapacitors based on 2D materials fulfill these requirements by having high specific capacitances for small active areas and masses. The charge storage mechanism in supercapacitors can be divided into two groups; (1) electric double-layer capacitors (EDLCs) and (2) pseudocapacitors. EDLCs store energy through the accumulation of ions at the interface between the electrode and the electrolyte, and because of this, their performance is dependent on the surface area of the electrode, pore size, and electrical conductivity.[20] Pseudocapacitors, on the other hand, use fast reversible redox reactions at the electrode−electrolyte interface, resulting in Faradaic charge transfer. EDLCs have the advantage of almost limitless cyclability with little degradation but comparatively low specific capacitances when compared to pseudocapacitors which have much higher specific capacitance but often suffer from performance degradation with repeated charge−discharge cycles.[21−23]

To enable comparison between different electrode materials, specific capacitance values are typically normalized by either the mass of the active material (F/g), the projected electrode area (mF/cm^2), or volume (F/cm^3). However, care should be taken

Received: May 28, 2015
Accepted: July 21, 2015
Published: July 21, 2015

DOI: 10.1021/acsami.5b04672
ACS Appl. Mater. Interfaces 2015, 7, 17388−17398

when comparing specific capacitance values reported in literature, as very low masses (μg) can give greatly overestimated values when extrapolated to the gram or even kilogram scale,[6,24] as well as excluding the contribution of conductive additives (such as carbon black) or binding agents. Because of the difficulties in scaling up specific capacitance values for very small masses (μg or mg) of active material to large scale (g or kg) applications, the use of area normalized capacitance (mF/cm^2) is regarded as more accurately scalable,[1,25,26] particularly for thin films of electrode material. The use of three-electrode systems can also exaggerate the performance of an electrode, more than doubling the measured capacitance and not accurately reflecting the performance of real world devices.[24,25] Thus, to accurately predict the performance of an electrode material, testing should be undertaken in a symmetrical two electrode system without any additives or binders.

Despite the increasing number of studies on the use of MoS_2 in supercapacitor electrodes, very little is understood about the fundamental electrochemical processes that contribute to its electron transfer characteristics and pseudocapacitance.[27,28] As well as Faradaic electron transfer resulting in the change in oxidation states of the Mo and S atoms at edge sites, several different non-Faradaic charge storage mechanisms have been proposed, including the adsorption of electrolyte ions onto the MoS_2 surface as well as the intercalation of ions between neighboring layers.[29−31] Previous work on thin layer graphene-based supercapacitors has reported a range of specific capacitances from 2 to 5 mF/cm^2 depending on the testing parameters, electrolyte, and electrode architecture.[32−34] However, there have been fewer published values for MoS_2 based devices but they range from 2 to 3.1 mF/cm^2 for solution exfoliated MoS_2 [31,35] and 8 mF/cm^2 for hydrothermally grown material.[31] Recently, the use of the metallic metastable 1T-MoS_2 phase was demonstrated to be an ideal supercapacitor electrode material due to its high conductivity combined with ion intercalation pseudocapacitance.[29] With the obvious benefits of these 2D materials it is possible to combine graphene with MoS_2 to produce highly efficient composite electrochemical supercapacitor devices. These composite devices are able to produce high gravimetric specific capacitances between 205 and 282 F/g.[36−38] Similar composites of graphene and metal oxides (e.g., MnO_2/graphene) have also been demonstrated previously, and these maximize the available pseudocapacitance of the oxide through the interconnectivity of both materials.[39−41]

In this work, we have produced few-layer (1−3 layers) MoS_2 by solution phase exfoliation; this was then combined with dispersions of exfoliated graphene to produce a MoS_2/graphene composite electrode material. The exfoliated graphene and MoS_2 were first characterized by a variety of techniques including optical absorption, Raman spectroscopy, as well as X-ray photoelectron spectroscopy (XPS) and scanning electron microscopy (SEM) to determine the quality of the electrode materials. Membranes of graphene and MoS_2 were formed by filtration of the dispersions and were characterized in symmetrical electrochemical coin cells with aqueous electrolytes to measure the charge storage behavior. Because of the inherent conductivity of the thin membranes, they can act as the active electrode without the need for any binding agents, simplifying device design while also reducing overall device weight. It was also possible to directly stack the membranes back-to-back, negating the need for a separate ion porous separator. It was found that while the individual materials had moderate specific capacitance values, the composite membranes had significantly improved values depending on the relative ratio of MoS_2/graphene, combined with excellent cyclability. Because of repeated ion intercalation and deintercalation that occurs with repeated cycling, the performance of the membranes increased significantly (up to 800%) with cycling, attributed to further exfoliation of the layered materials. The improved performance of the composite electrodes is attributed to the decreased resistance from the incorporated graphene flakes combined with the increased surface area created by the stacking interactions of the MoS_2 and graphene flakes. These results indicate that composites of 2D materials can be integrated into highly efficient energy storage applications, which with further optimization should be suitable for widespread applications.

EXPERIMENTAL SECTION

MoS_2 Dispersion Preparation. MoS_2 dispersions were created by liquid phase exfoliation as has been reported previously.[18,19,42] Briefly, MoS_2 powder (10 mg/mL) was dispersed in *N*-methyl-2-pyrrolidone (NMP) and ultrasonically processed in a bath sonicator (Elmasonic P70H) operating at 37 kHz and 40% amplitude for 12 h while cooling to maintain a stable temperature of 20 °C. After this sonication, the dispersions were centrifuged at 6000 rpm (3139*g*) for 30 min to remove any unexfoliated material, the supernatant was then decanted and fresh solvent added before repeating the centrifugation to ensure a narrow distribution of flake dimensions and thickness. The resultant MoS_2 suspensions were stable in solution for several months with no detectable sedimentation.

Graphene Dispersion Preparation. Graphene powder (Grat-G1L, BGT Materials, U.K.) was dispersed in NMP (10 mg/mL) before sonicating briefly (20 min) to ensure a homogeneous suspension. This graphene dispersion was then centrifuged twice at 6000 rpm (3139*g*) for 30 min, as performed for the MoS_2, to ensure that no unexfoliated material remained. The resultant graphene suspensions were also stable in solution for several months with almost no detectable sedimentation.

Raman Spectroscopy and Photoluminescence. To ascertain the MoS_2 and graphene layer number, the dispersions were deposited onto a Si/SiO_2 (300 nm thickness of oxide) wafer and the solvent was removed by heating on a hot plate allowing flakes to be identified by optical microscopy and Raman spectroscopy. Confocal Raman spectroscopy and photoluminescence measurements were conducted using a Renishaw inVia microscope with a 532 nm (2.33 eV) excitation at a power of 1 mW with a 100× objective and a grating of 1800 l/mm to achieve a spectral resolution of ∼1 cm^{-1}.

Membrane Preparation. Films of the exfoliated MoS_2 and graphene, as well as mixtures of both, were synthesized by first diluting the NMP dispersions in isopropanol (IPA) by a factor of 20 followed by filtering through preweighed PVDF filters with 0.1 μm pore size. These were then washed with IPA to remove any NMP residue and dried in an oven at 80 °C to remove any residual solvent. The mass of active material used was determined by weighing the membrane after drying and kept at ∼0.75 mg (mass loading: 1 mg/cm^2). The MoS_2, graphene, and composite films were then each analyzed by Raman spectroscopy, XPS, SEM, and electrochemistry.

Electrochemistry. Cyclic voltammetry (CV), electrochemical impedance spectroscopy (EIS), and galvanostatic charge/discharge (GCD) were performed using a PGSTAT302N potentiostat (Metrohm Autolab, The Netherlands). All electrochemical measurements were performed using a sealed symmetrical coin cell (CR2032). The membranes were stacked back-to-back within the coin cell with the active material making direct contact with the current collector. The electrolyte used was aqueous 1 M Na_2SO_4. Cyclic voltammetry was performed at scan rates ranging from 5 to 1000 mV/s. EIS was performed at a frequency range of 0.1 Hz to 100 kHz with a 10 mV (rms) perturbation and 0 V dc bias.

DOI: 10.1021/acsami.5b04672
ACS Appl. Mater. Interfaces 2015, 7, 17388−17398

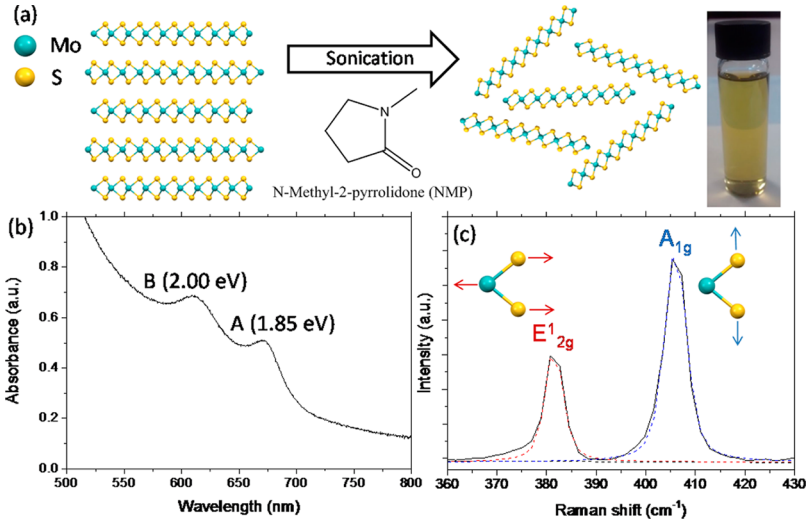

Figure 1. (a) Illustration showing the crystal structure of MoS_2 and the sonication process along with a photograph showing the stable MoS_2 dispersion in NMP after centrifugation. (b) Optical absorption spectrum of MoS_2 dispersion in NMP showing the A and B excitonic absorptions. (c) Raman spectrum of solution exfoliated MoS_2 flake supported on SiO_2. The main Raman peaks are labeled and the vibrations shown schematically.

Scanning Electron Microscopy. Scanning electron microscope (SEM) analysis was performed on a FEI/Philips XL30 E-SEM under high vacuum conditions with an accelerating voltage of 15 kV. All images were taken using the secondary electron detector.

X-ray Photoelectron Spectroscopy. X-ray photoelectron spectroscopy (XPS) was performed at the EPSRC NEXUS facility (Newcastle, U.K.) using an AXIS Nova spectrometer (Kratos Analytical, U.K.) which utilizes a monochromatic Al Kα source operated at 225W (15 kV and 15 mA) with an analysis area of 300 μm × 700 μm, and three points were analyzed on each sample. Survey spectra were collected at a pass energy of 160 eV and were the average of three sweeps, while high resolution spectra were collected at a pass energy of 20 eV and were the average of 10 sweeps. Charge neutralization was used for all samples.

RESULTS AND DISCUSSION

Synthesis and Characterization of Electrode Membranes. To understand the performance of any energy storage devices based on MoS_2 flakes, it is paramount to first thoroughly characterize the active material. As shown in the schematic of Figure 1a, dispersions of MoS_2 were prepared by solution phase exfoliation of bulk MoS_2 powder by ultrasonication in *N*-methyl-2-pyrrolidone (NMP). Because of the relatively weak interlayer van der Waals interactions binding the MoS_2 layers, exfoliation down to a few layers or monolayers by ultrasonication in the correctly chosen solvent is possible. NMP was chosen, as it has been shown to be highly efficient at exfoliating MoS_2 as well as maintaining a stable dispersion.[18,19,42] As the bulk powder is reduced in thickness down to a few layers (1−3), it is stabilized in solution and prevented from reaggregation due to the close match in surface energy between the MoS_2 layers and the solvent. This close match in surface energy between the MoS_2 flakes and solvent causes the enthalpy of mixing to be small, ensuring a stable dispersion.[18,19,42] The optical image in Figure 1a shows the stable MoS_2 dispersion in NMP with no discernible sedimentation over extended periods of time. Figure 1b shows the absorption spectrum of the MoS_2 dispersion with two clear excitonic absorptions at 1.85 and 2 eV labeled A and B, respectively. The lack of any convolution of these two excitonic absorptions indicates a lack of damage or disorder that may have occurred because of the ultrasonication process.[43] This indicates that solution exfoliation does not significantly damage the crystal structure.

Figure 1c shows the Raman spectrum of an exfoliated MoS_2 flake after a drop of the dispersion was drop cast, after further dilution, onto a silicon wafer (Si/SiO_2) to allow easy identification by optical microscopy. The two characteristic Raman peaks for MoS_2 are labeled the in-plane vibration (E^1_{2g}) and the out-of-plane (A_{1g}).[44,45] The wavenumber of these peaks, as well as peak separation, can be used to determine the number of MoS_2 layers. Typically the Raman spectrum of micromechanically exfoliated MoS_2 crystals exhibits a peak separation of ∼20 cm^{-1} while bulk MoS_2 has a separation of ∼25 cm^{-1}, as well as the full width at half-maximum (fwhm) of the peaks increasing with decreasing layer number.[44,45] When we compare the Raman spectrum of the raw powder and the exfoliated flakes of MoS_2 (Supporting Information, Figure S1), we see a significant shift due to the sonication process indicating that the resultant flakes are few layer (1−3 layers). The flake size and thickness are dependent on both the sonication time used and also the postprocessing such as centrifugation speed and duration.[42] Thus, these parameters can be easily tuned to produce films with the appropriate dimensions. We also see a significant difference when we compare the spectrum of the bulk crystal compared to the raw powder (Figure S1), where the peak frequencies are downshifted for the powder as well as significantly broader. This indicates that the powder is much more disordered than the bulk material, as may be expected. By varying the crystallinity of the starting material, it may be possible to reduce the distribution of the lateral flake size and thickness as needed for a specific application. Because of the semiconducting nature of MoS_2, we can also measure the photoluminescence (PL) of the bulk starting materials and compare this to the exfoliated material as seen in the Supporting Information (Figure S2) which shows a clear shift in electronic structure due to the reduction in thickness. Because of the large numbers of flakes in any given dispersion, there exists a distribution of thicknesses and also lateral sizes with monolayer flakes observed as well as thicker flakes. SEM analysis, seen in the Supporting Information (Figure S3), of the membrane formed after filtration shows an MoS_2 "paper" made up of many small

DOI: 10.1021/acsami.5b04672
ACS Appl. Mater. Interfaces 2015, 7, 17388−17398

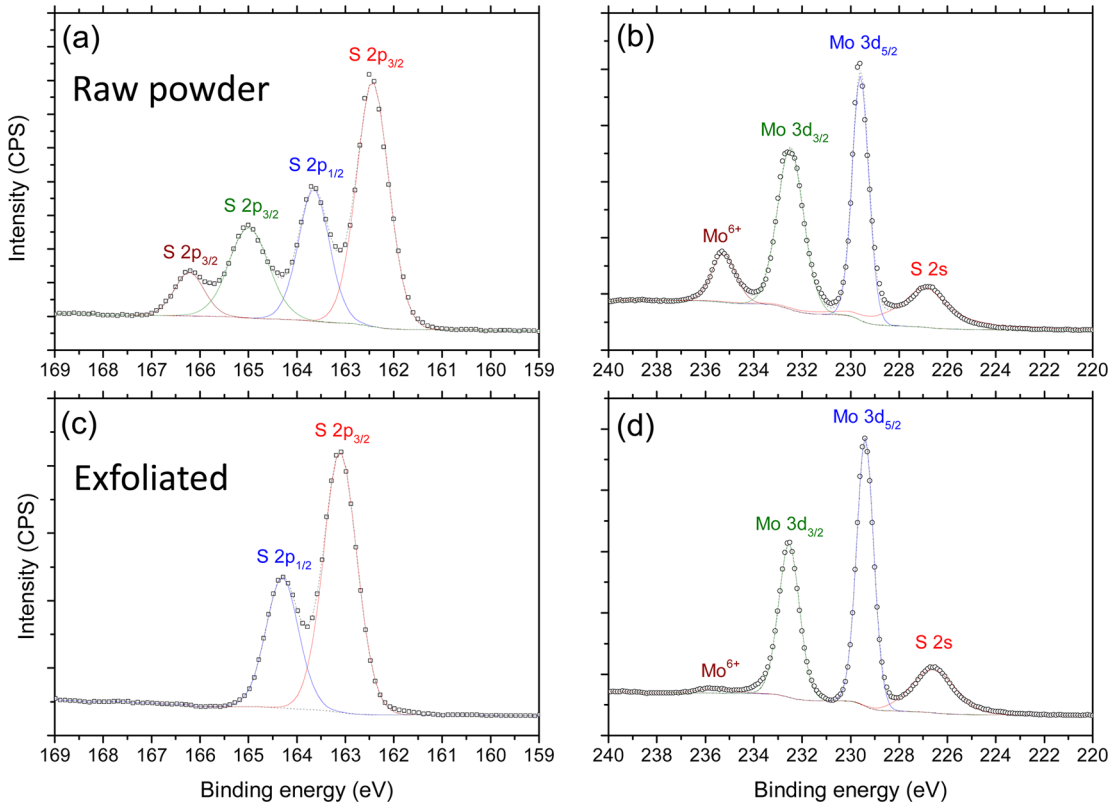

Figure 2. High resolution XPS spectra of MoS_2 raw powder showing the S 2p (a) and Mo 3d (b) binding regions. The suborbital splitting is labeled. The same binding energy regions are shown for the solution exfoliated material in (c) and (d).

individual flakes that are stacked horizontally on top of one another. The individual lateral flake size can be seen to range from 200 nm up to 1 μm; this is in agreement with literature values for flakes prepared under similar conditions.[19,42]

To investigate the chemical state of the MoS_2 films, XPS was performed on the raw powder and the exfoliated flakes. Previously, it has been shown that XPS can be used to determine the coordination of the molybdenum atoms to distinguish between the different phases that exist, either trigonal prismatic in the case of 2H-MoS_2 or octahedral for 1T-MoS_2.[12,43] XPS can also be used to determine the purity of the starting material, which can greatly affect the subsequent performance in electrochemical energy storage devices, e.g. presence of redox active contaminants. First, wide-scale survey spectra were taken over a large range of binding energies to determine the presence of different elements (Supporting Information Figure S4). As expected, the only elements present were molybdenum, sulfur, as well as adventitious carbon and oxygen. As well as the wide-scale spectra, high resolution spectra were taken of the main elements; Figure 2 shows the sulfur 2p (S 2p) and the molybdenum 3d (Mo 3d) shells for the raw MoS_2 powder (Figure 2a,b) and the film after exfoliation (Figure 2c,d). When we compare the spectra for the raw powder and the exfoliated films, we can see a clear difference. In particular the sulfur 2p typically splits into two components in MoS_2 (S $2p_{1/2}$ and the S $2p_{3/2}$); however, in the raw powder four separate peaks are resolved indicating that the sulfur atoms are in two different chemical states. This is likely caused by the partial oxidation of the MoS_2 into MoS_xO_y at edges and defect sites; this is supported by the molybdenum spectra shown in Figure 2b where we see the expected Mo $3d_{5/2}$ and Mo $3d_{3/2}$ as well as a third peak at ~236 eV which can be attributed to molybdenum (Mo^{6+}) in an octahedral configuration, which is typically observed in partially oxidized MoS_2.[46−48] After exfoliation the XPS spectra of the film change significantly with both the S 2p (Figure 2c) and Mo 3d (Figure 2d) regions representing the expected spectra for pristine 2H-MoS_2.[43,46] We can see in Figure 2d that a small peak still remains at ~236 eV, and this indicates that a very small amount of surface oxide is still present; however, the intensity is greatly reduced from that of the starting material. This result indicates that the solution phase exfoliation removes any surface oxides that have formed on the MoS_2 powder as well as removes any amorphous or contaminated material.

To enhance the performance of the semiconducting 2H-MoS_2, we have produced composites of MoS_2 and graphene in differing ratios and characterized the resulting membranes by Raman and XPS before electrochemical testing. Composite membranes were synthesized by mixing dispersions of MoS_2 and graphene in differing weight ratios: 1:1, 1:3, 3:1 (MoS_2/graphene). The performance of each of these composite membranes was then compared to the respective "pure" membranes (data not shown). It was found that each of the composites had improved performance over the pure membranes, but the 1:3 composite membranes exhibited the highest specific capacitance, and so we will focus on this ratio. The superior performance of the 1:3 ratio composite is attributed to the balance between the high concentration of highly conductive graphene combined with a smaller amount of MoS_2 flakes to prevent restacking and provide extra surface area. Commercially available graphene powder was utilized and first characterized by Raman and XPS before use, as discussed further in the Supporting Information (Figure S5). The graphene was found to consist of flakes that are approximately

DOI: 10.1021/acsami.5b04672
ACS Appl. Mater. Interfaces 2015, 7, 17388−17398

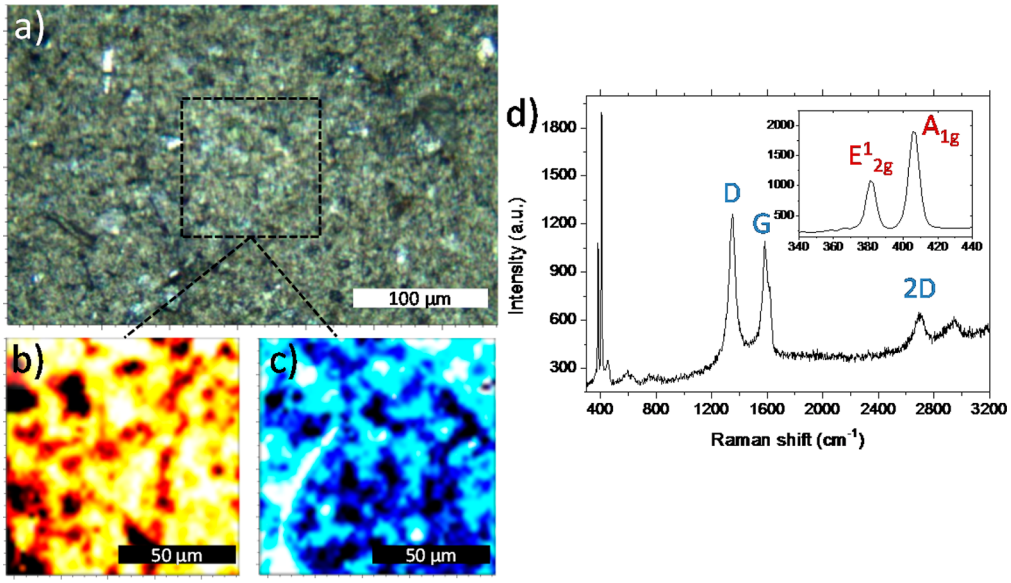

Figure 3. (a) Optical image (×100 magnification) of composite membrane (MoS_2/graphene ratio, 1:3) supported on PVDF filtration membrane. Raman maps showing distribution of MoS_2 A_{1g} intensity (b) and graphene G band intensity (c) within the composite. (d) Raman spectrum of composite membrane showing both the MoS_2 peaks (enlarged in inset, E^1_{2g}, 381 cm^{-1}; A_{1g}, 405 cm^{-1}) and graphene peaks (D, 1348 cm^{-1}; G, 1582 cm^{-1}; 2D, 2700 cm^{-1}).

3−5 μm in length, with thicknesses of a few layers (1−3). XPS analysis indicated that some residual contaminants from the exfoliation process remained; however, these were removed after dispersing into NMP and depositing onto the substrate. Membranes of the graphene were created in the same fashion as for the MoS_2 and composites, and each was characterized separately.

To determine the distribution of MoS_2 and graphene within the composite membranes we can use Raman spectroscopy to take a map over a large area. These confocal Raman maps are created by taking spectra every 0.5 μm in a raster pattern over a selected area. The intensity of a given peak can then be plotted visually, and used to determine the spatial distribution within the membrane. Figure 3a shows the optical photograph of one of the composite membranes, using a 100x objective. The high surface roughness seen is ideal for thin layer supercapacitor devices, although some highly reflective larger restacked flakes are visible and the performance of the membrane could be further improved by minimizing these large aggregates. The area shown by the square was then mapped and the corresponding maps are shown in Figure 3b (MoS_2, A_{1g} intensity) and Figure 3c (graphene, G band intensity). From these maps we can see that both the MoS_2 and graphene are homogeneously distributed throughout the membrane, even the darker areas of the maps represent only a minimum in the signal not an absence of either material. At all areas measured there was a combination of both graphene and MoS_2 signal. This indicates that during the mixing of the each of the dispersions and subsequent membrane formation, the two materials are thoroughly mixed and evenly distributed. Figure 3d shows a representative Raman spectrum taken from the composite membrane, showing both the characteristic MoS_2 peaks and the graphene peaks as labeled.

To further investigate the morphology of each membrane, SEM analysis was performed, and typical SEM images of each membrane composition are shown in Figure 4. Figure 4a shows the graphene membrane, and we can clearly see that it consists of many large sheets (3−5 μm) forming a highly wrinkled

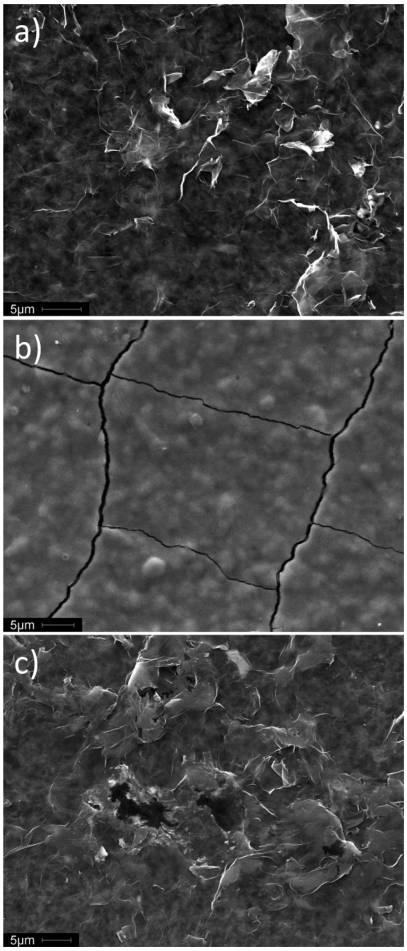

Figure 4. SEM images of the graphene membrane (a), MoS2 membrane (b), and the composite (1:3) membrane (c). The scale bar in each image is 5 μm.

DOI: 10.1021/acsami.5b04672
ACS Appl. Mater. Interfaces 2015, 7, 17388−17398

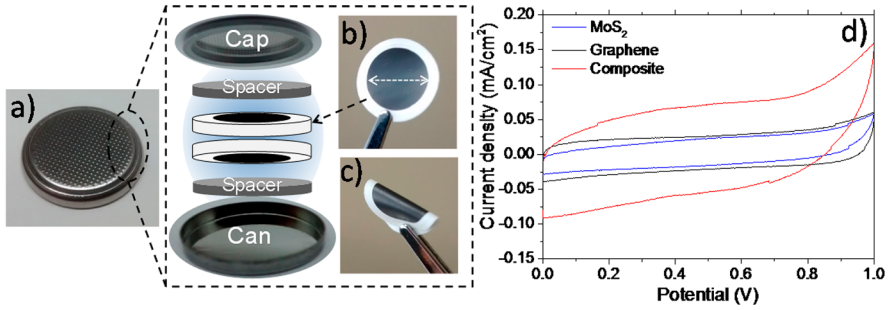

Figure 5. (a) Photograph of assembled symmetrical coin cell (CR2032). Exploded view schematically shows the internal construction. Stainless steel spacers are inserted to ensure good electrical contact directly between the active material and the outer electrode. The PVDF membranes themselves act as the ion transporting spacers. (b, c) Photographs of PVDF supported membrane formed from exfoliated MoS_2 (mass loading of 1 mg/cm^2, scale bar is 13 mm). (d) Plot comparing the cyclic voltammograms (CVs) of the symmetrical coin cells constructed from MoS_2 (blue), graphene (black), and composite membranes (1:3) showing the increased capacitance of the composite membrane. Scan rate is 50 mV/s, and the electrolyte is aqueous 1 M Na_2SO_4.

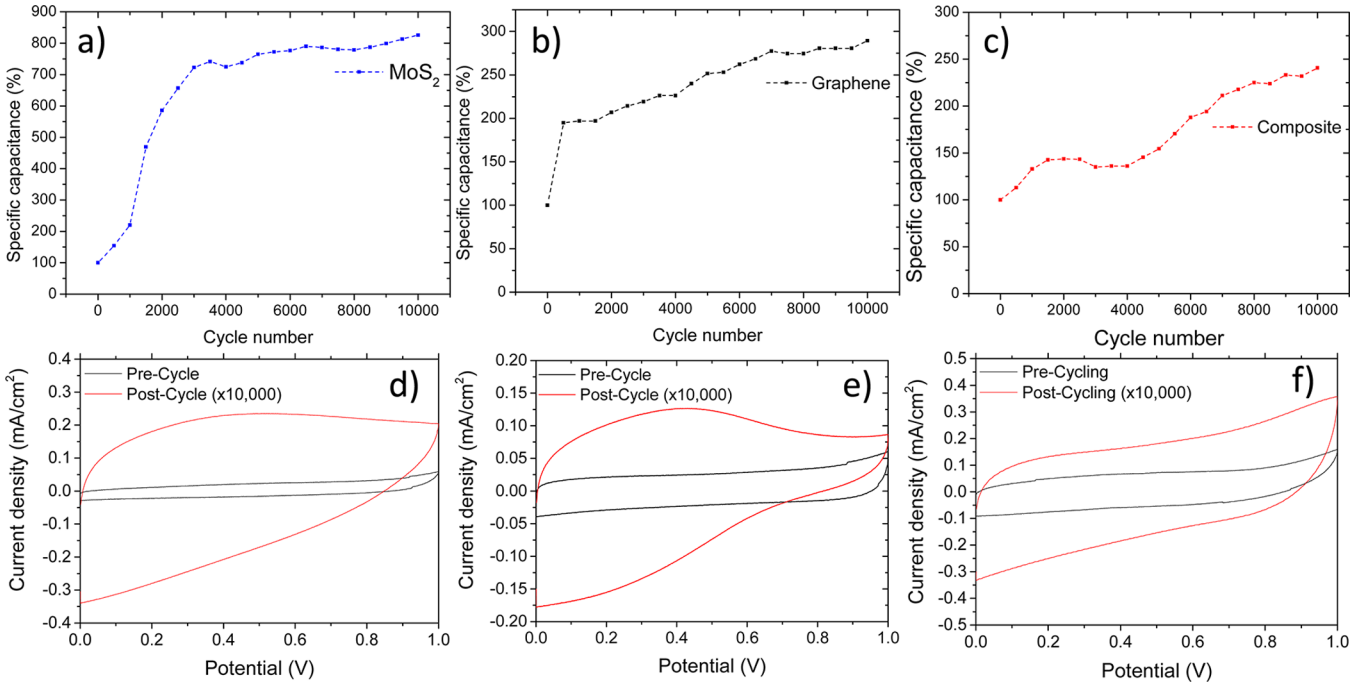

Figure 6. Plot of specific capacitance change (%) with continued charge/discharge cycles (current density of 1 mA/cm^2) for the symmetrical MoS_2 cell (a), graphene cell (b), and composite (1:3) membrane cell (c). In each case there is a large increase in specific capacitance with continued cycling before stabilization. The CVs (scan rate of 50 mV/s) precycle and post 10 000 cycles are shown for MoS_2 (d), graphene (e), and the composite (f).

surface. Figure 4b shows the MoS_2 membrane, and because of the smaller flake size (0.2−1 μm), this forms a smoother continuous film with several cracks formed due to manipulation during the sample preparation. The composite film is seen in Figure 4c, and because of the combination of the larger graphene sheets and the smaller MoS_2 flakes, we observe a rougher surface with increased surface area compared to either of the "pure" membranes. Smaller individual MoS_2 flakes are also visible stacked on top of the larger graphene sheets. From the high resolution images shown in the Supporting Information (Figure S3) we can also see that the thickness of these films is on average ∼0.5 μm.

Electrochemistry. After thorough characterization of the MoS_2 suspensions and resulting films, electrochemical testing was carried out in a symmetrical coin cell architecture (CR2032), as seen in Figure 5a. Individual electrodes were produced by filtering the suspension of exfoliated material through a preweighed polyvinylidene fluoride (PVDF) filter to form a MoS_2 membrane, without any additional polymeric binders or conductive additives. Approximately 0.75 mg (mass density of 1 mg/cm^2) of exfoliated MoS_2 was used as the active material (an optical image of one of the MoS_2 membranes can be seen in Figure 5b). These flexible membranes were then stacked back-to-back within the cell, with the supporting membranes themselves acting as the ion porous charge separator and providing direct electrical contact between the current collector and the active material. The electrolyte used in this work was aqueous 1 M Na_2SO_4; a pH neutral electrolyte was used to avoid side reactions such as hydrogen evolution, increasing the long-term stability of the membrane. However, because of the relatively large size of the solvated electrolyte ions, when compared to strong acidic or basic electrolytes, the specific capacitance of Na_2SO_4 can be more than 10 times lower than for H_2SO_4.[30] To act as a comparison, the

DOI: 10.1021/acsami.5b04672
ACS Appl. Mater. Interfaces 2015, 7, 17388−17398

performance of a MoS_2 coin cell with 1 M H_2SO_4 can be seen in the Supporting Information (Figure S6); the current density is seen to be ~10 times higher than the neutral electrolyte. However, hydrogen evolution occurs when the potential is increased, as MoS_2 has been shown to be an excellent H_2 evolution catalyst.[9,12,49] This H_2 evolution severely limits the lifetime of the coin cell because of deformation of the cell with increasing gas pressure. It has also been demonstrated previously that the potential window can be extended up to 1.6 V with the use of sodium sulfate (Na_2SO_4) as the electrolyte, because of the higher overpotential for the electrolysis of water.[50] Organic electrolytes allow for a large potential window to be used when testing supercapacitor electrodes, as they are not limited by the electrolysis of water which limits the operating potential of aqueous devices to ~1 V.[6,24] However, organic electrolytes are hampered by low conductivity and bulky ions, as well as sensitivity to contamination from atmospheric moisture.

Figure 5d compares the cyclic voltammograms (CV) of the MoS_2 membranes as well as a graphene film and a composite of both graphene and MoS_2. The response of the cell shows a typical "square" EDLC response for each of the membranes. When the three membranes are compared, the composite shows a significantly improved performance over either of the individual components. One key drawback to pure MoS_2 based supercapacitors is the inherent resistivity of the films when compared to carbon based devices. Conductivity of the film can be increased by mixing of graphene and MoS_2 together to form composites while also exploiting the inherent capacitance of graphene. Several examples of such composites have been demonstrated previously, where it is shown that the addition of conductive material increases the specific capacitance.[36,38,51]

Cycling Stability. One of the most important metrics for comparing supercapacitor electrodes is the cycling stability. Ideal EDLC supercapacitors should possess extremely high stability with minimal degradation in performance with repeated charge/discharge cycles, while pseudocapacitors typically sacrifice cycling stability for increased energy density.[4] Typically when graphene or MoS_2 supercapacitor electrodes are cycled continuously, there is a gradual degradation in capacitance due to increased resistance between flakes, collapse of the porous structure, as well as desorption of active material from the current collector. Thus, the cycling stability is a good indication of the material's suitability for real world supercapacitor applications. Previously, reported literature values for graphene supercapacitor cycling stability vary depending on the testing conditions but can range from 30% loss to almost no loss after 10 000 cycles.[1] This is compared to a 30% decrease in capacitance for solution exfoliated MoS_2 after only 200 cycles[35] and an 8% decrease over 1000 cycles for laser patterned MoS_2.[31]

Figure 6 shows the cycling stability of the MoS_2 (Figure 6a), graphene (Figure 6b), and composite (Figure 6c) membranes over 10 000 charge/discharge cycles at a current density of 1 mA/cm^2. The intermediate discharge cycles (every 2000 cycles) are shown for each membrane in the Supporting Information (Figure S10). In the case of the MoS_2 membrane (Figure 6a) instead of a gradual degradation of the specific capacitance with repeated cycling as seen typically for such devices,[35,36,52] there is an initial large increase (800%) in the performance over the first ~3000 cycles before stabilizing for the remaining 7000 cycles. Upon assembly electrochemical cells require "preconditioning" (several charge/discharge cycles) to ensure the electrolyte has permeated throughout the porous structure and the cell has stabilized.[24] For all results presented here each system was preconditioned by charging/discharging for ~200 cycles (1 mA/cm^2) prior to further characterization. Thus, the observed increase with repeated cycling only occurs when >1000 charge/discharge cycles are applied. An approximate doubling of the specific capacitance (10 mF/cm^2) is measured for the graphene membrane (Figure 6b) over the first ~500 cycles, after which the performance increases only slightly over the remaining cycles. The composite membrane exhibits a different behavior, increasing gradually over the duration to ~250% of the initial value (11 mF/cm^2) after 10 000 cycles. The lack of any decrease with continued cycling demonstrates the applicability of these membranes to devices.

The large initial increase in capacitance of the MoS_2 membrane can be attributed to a combination of (1) a transition in the charge storage mechanism from EDLC to pseudocapacitive ion intercalation and deintercalation, combined with (2) increased active surface area due to partial exfoliation. Initially the predominant charge storage mechanism of the MoS_2 membrane is accumulation of ions at the double-layer interface between the flakes and the electrolyte, as indicated by the shape of the CV plot (seen in Figure 5d). However, during charging alkali metal ions present in the electrolyte (Na^+) can adsorb onto the surface and intercalate between the MoS_2 layers of the membrane, represented by eq 1.

$$MoS_2 + Na^+ + e^- \leftrightarrow MoS{-}SNa \quad (1)$$

This ion intercalation pseudocapacitance has been observed previously for MoS_2 films[29−31,37] and particularly for transition metal oxide films.[22,53−55] The continual intercalation and deintercalation of the relatively large sodium ions over repeated cycles can also lead to exfoliation of the layers that are restacked during the filtration process,[56,57] leading to an increased surface area and subsequently a much larger specific capacitance. Layered materials such as MoS_2 are unique in that their structure allows for this dynamic expansion to allow ions to intercalate without damage to the lattice occurring.[29] This transition in charge storage mechanism can be seen when comparing the CV plots before and after cycling, as seen in Figure 6d, which show that after cycling the current has increased significantly, but the shape of the plot is less ideal, indicative of pseudocapacitive Faradaic charge transfer.[21,22] Further evidence of this partial exfoliation can be seen in the SEM analysis shown in the Supporting Information (Figure S11), where we see that after cycling the MoS_2 membrane exhibits increased surface roughness. The graphene membrane also shows an increase in capacitance (Figure 6b) after cycling, and more noticeable is the change in shape of the CV plot (Figure 6e). Because of its high conductivity, the precycle CV plot displays highly ideal double-layer charge storage, as expected from graphene.[4,58] After cycling there is an increase in capacitance of ~250%; again the shape of the CV curve after cycling indicates pseudocapacitive behavior. This increased capacitance with continuous cycling has been reported previously for reduced graphene oxide films and was also attributed to the partial exfoliation with continued ion intercalation/deintercalation increasing the active surface area, termed "electroactivation".[33,59,60]

Finally, the composite membrane (Figure 6c) shows a moderate steady increase with cycling duration up to ~250%. When we compare the CV data before and after the cycling

DOI: 10.1021/acsami.5b04672
ACS Appl. Mater. Interfaces 2015, 7, 17388−17398

(Figure 6f), we see that the response indicates highly ideal EDLC behavior when compared to the pure membranes in Figure 6d and Figure 6e. This indicates that the composite of both graphene and MoS_2 together is better able to resist structural changes that occur with continual charge and discharge cycles. Typically, when dispersions of 2D materials are deposited into a film, the van der Waals attraction between neighboring sheets causes restacking to occur, and this limits the available surface area, thus reducing the specific capacitance. Thus, it is deduced that differences in flake dimensions and surface energy in the case of the MoS_2/graphene composites form disordered heterostructures and prevent restacking, as seen previously in the SEM analysis (Figure 4). It is this physical prevention of restacking, effectively increasing the specific surface area, that is likely responsible for the ideal EDLC charge storage behavior observed.

Specific Capacitance of Thin-Layer Membranes. The specific capacitance (C_{sp}) of the membranes can be calculated from the CV plots using eq 2.[1]

$$C_{sp} = \frac{\int I(V)\, dv}{vA\,\Delta V} \quad (2)$$

where $\int I(V)$ is equal to the integrated area under the CV plot, v is the scan rate, A is the electrode area, and ΔV is the potential window. Figure 7 plots the calculated specific capacitance with increasing scan rates for each of the three membranes before and after cycling. (The CV plots showing the increasing potential scan rates are shown in the Supporting Information, Figure S7–S9.) As expected from eq 2, there is a decrease in specific capacitance with increasing scan rate, due to the transport limit on the supply of ions. As discussed previously, the graphene displays ideal EDLC behavior before cycling, and this is also supported by the high discharge rate as the scan rate increases, with the specific capacitance decreasing by only 43% when increasing the scan rate from 5 mV/s (1.16 mF/cm^2) up to 1000 mV/s (0.66 mF/cm^2). The MoS_2 membrane, however, displays very high specific capacitance at low scan rates (1.83 mF/cm^2 at 5 mV/s) but decreases by 80% at 1000 mV/s to 0.37 mF/cm^2, which is indicative of pseudocapacitive behavior.[30] These capacitance values correlate well with reported values for solution exfoliated MoS_2 films that were able to produce ~2 mF/cm^2 at 10 mV/s.[35] The composite membrane exhibits much larger specific capacitance than either of the single component membranes; the specific capacitance was measured as 4.29 mF/cm^2 at 5 mV/s; however, the composite suffers from the same degradation as seen in the pure MoS_2 membrane with increasing scan rate, decreasing by ~80% at 1000 mV/s to 0.98 mF/cm^2. This larger specific capacitance precycling is attributed to physical interactions between the MoS_2 and graphene flake, preventing restacking from occurring and increasing the active surface area. As well as the area normalized specific capacitances, values for the gravimetric and volumetric capacitance are provided in the Supporting Information (Table S1–S2) to allow for comparison to other similar works.

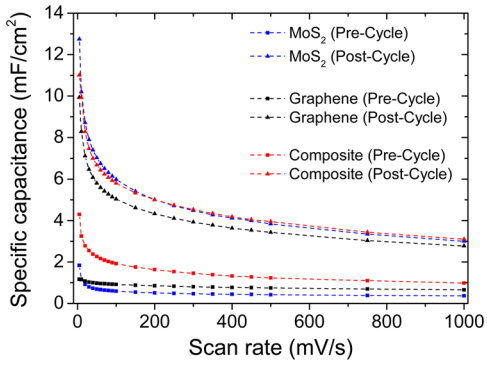

Figure 7. Plot of specific capacitance (mF/cm^2) with increasing scan rate calculated from cyclic voltammetry for each cell before and after cycling 10 000 times (seen in Figure 6).

The postcycle specific capacitance increases significantly for all three membrane systems, attributed to "electroactivation" as discussed previously, and the performance of the MoS_2 and composite membranes are seen to match one another closely. This is surprising, as the composite membrane consists of just 25 wt % of MoS_2 compared to the pure membrane but is able to match its performance. The specific capacitance of the composite membrane ranges from 11 mF/cm^2 (5 mV/s) down to 3.1 mF/cm^2 (1000 mV/s). These specific capacitance values compare favorably with values published previously, ranging from 2 to 3.1 mF/cm^2 for solution exfoliated MoS_2.[31,35] The specific capacitance of the composite also compares favorably to graphene/nanotube composites, which generated 2.16 mF/cm^2.[32] As well as cyclic voltammetry, galvanostatic charge/discharge at different current densities was used to calculate the specific capacitance of each of the membranes (see Supporting Information, Figure S7–S9), and the values were seen to correspond closely to those calculated from CV. Electrochemical impedance spectroscopy (EIS) was also used to investigate the frequency response of the coin cells before and after cycling (Supporting Information, Figure S12–S13), supporting the transition in charge storage mechanism from EDLC to pseudocapacitance. From the EIS analysis we can also determine the equivalent series resistance (ESR) within the cells, with the MoS_2 membrane having the highest ESR of 1.6 Ω and lower for the composite (0.7 Ω) and pure graphene (0.96 Ω).

Self-Discharge Behavior. Although very important when discussing application of supercapacitor designs, the self-discharge behavior is often neglected when characterizing the performance of a given material.[4,25] Self-discharging of supercapacitors can severely limit their applicability to real world applications and thus are an important figure of merit when comparing electrode designs. The spontaneous voltage decrease that occurs within a charged supercapacitor under open circuit conditions, often referred to as self-discharge, can occur because of three mechanisms: Faradaic processes, leakage current, and charge redistribution.[61,62] These Faradaic processes that can occur, when aqueous electrolyte solutions are used, are thought to be predominantly oxygen reduction at the negative electrode.[63] Leakage current occurs when charged ions or impurities within the electrolyte spontaneously migrate from each electrode, thereby reducing the cell potential.[62] Charge redistribution occurs when selective areas of the active material are unevenly charged, leading to areas that are overcharged while others have lower charge. This charge redistribution between these areas then leads to an overall decrease in cell potential. Thus, when a supercapacitor electrode material is characterized, minimizing the self-discharge rate is important to maximize performance. In the case of EDLC devices the voltage decreases initially from its initial value quickly and the rate decreases with time.[61] Over this initial rapid decrease in potential the device is exhibiting

DOI: 10.1021/acsami.5b04672
ACS Appl. Mater. Interfaces 2015, 7, 17388–17398

noncapacitive behavior (due to Faradaic processes and charge redistribution); after this the linear decrease in potential is typical of a dielectric capacitive response due to current leakage.[61] The rate of self-discharge has also been shown to be strongly dependent on the charging duration as well as method (galvanostatic and potentiostatic).

Figure 8 plots the open-circuit voltage of each of the three symmetrical cells (postcycling); each underwent 15 min of potentiostatic charging to 1 V before the open-circuit potential was measured over 1 h. It can be seen that the graphene membrane (black) suffers from the highest rate of self-discharge, followed closely by the MoS_2 membrane (blue). The composite membrane (red), however, displays much better charge retention (37% greater than the graphene, 25% greater than MoS_2). The increased charge retention performance of the composite membrane indicates that the synergistic effect of combing the highly conductive graphene with the pseudocapacitive MoS_2 allows for reduced Faradaic leakage and charge redistribution across the membrane.

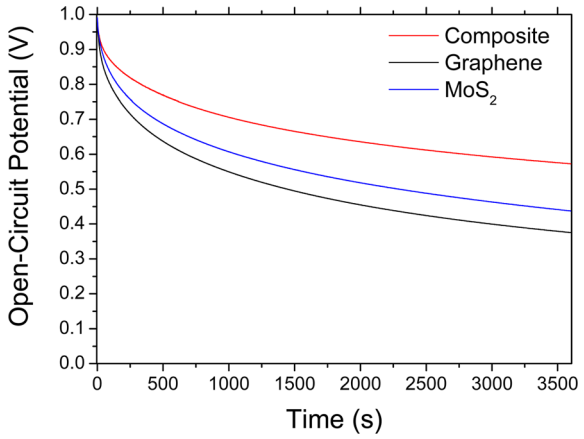

Figure 8. Self-discharge behavior for the symmetrical graphene cell (black), MoS_2 cell (blue), and composite cell (red). The cells each underwent potentiostatic charging at 1 V for 15 min prior to measuring the open-circuit potential.

CONCLUSION

We have demonstrated that composite membranes made from solution exfoliated dispersions of 2D materials, such as semiconducting MoS_2 and semimetallic graphene, can create a synergistic effect that allows for high performance electrochemical energy storage devices to be constructed. The high specific capacitance of the MoS_2/graphene membranes, with only a small mass loading (~1 mg/cm^2), no added binders, and no extra porous charge separators, demonstrates a cheap, simple, and scalable electrochemical energy storage cell architecture with excellent cycle life. It was found that the optimal ratio of the MoS_2 and graphene, in terms of electrochemical performance, was 1:3 (MoS_2/graphene). The composite membrane was able to achieve a high specific capacitance (~11 mF/cm^2 at 5 mV/s). With continued cycling it was observed that electroactivation due to ion intercalation leads to a significant increase in specific capacitance. The self-discharge behavior also demonstrated that the composite membrane possessed superior charge retention compared to the individual components. This work suggests that composites of various 2D materials (TMDs, graphene, hBN, etc.) can easily be combined and used to enhance the performance of single component materials for electrochemical energy storage.

ASSOCIATED CONTENT

Supporting Information

The Supporting Information is available free of charge on the ACS Publications website at DOI: 10.1021/acsami.5b04672.

Raman comparison of powder and single-crystal MoS_2 flakes, Raman maps of composite membranes, further SEM analysis, comparison of electrolytes, Raman and XPS characterization of graphene powder, galvanostatic charge/discharge curves, and electrochemical impedance spectroscopy for coin cell devices (PDF)

AUTHOR INFORMATION

Corresponding Authors

*M.A.B.: e-mail, Mark.Bissett@manchester.ac.uk.
*R.A.W.D.: e-mail, Robert.Dryfe@manchester.ac.uk.

Author Contributions

All authors have given approval to the final version of the manuscript.

Notes

The authors declare no competing financial interest.

ACKNOWLEDGMENTS

The authors acknowledge funding from BGT Materials, U.K., as well as the EPSRC (Grant ref EP/K016954/1). The authors also thank Anders J. Barlow at the National EPSRC XPS User's Service (NEXUS) at Newcastle University for assistance acquiring the XPS data.

REFERENCES

(1) Xiong, G.; Meng, C.; Reifenberger, R. G.; Irazoqui, P. P.; Fisher, T. S. A Review of Graphene-Based Electrochemical Microsupercapacitors. *Electroanalysis* **2014**, *26* (1), 30−51.
(2) Liu, C.; Yu, Z.; Neff, D.; Zhamu, A.; Jang, B. Z. Graphene-Based Supercapacitor with an Ultrahigh Energy Density. *Nano Lett.* **2010**, *10* (12), 4863−4868.
(3) Huang, Y.; Liang, J.; Chen, Y. An Overview of the Applications of Graphene-Based Materials in Supercapacitors. *Small* **2012**, *8* (12), 1805−1834.
(4) Chen, J.; Li, C.; Shi, G. Graphene Materials for Electrochemical Capacitors. *J. Phys. Chem. Lett.* **2013**, *4* (8), 1244−1253.
(5) Raccichini, R.; Varzi, A.; Passerini, S.; Scrosati, B. The Role of Graphene for Electrochemical Energy Storage. *Nat. Mater.* **2015**, *14*, 271−279.
(6) Simon, P.; Gogotsi, Y. Capacitive Energy Storage in Nanostructured Carbon−Electrolyte Systems. *Acc. Chem. Res.* **2013**, *46* (5), 1094−1103.
(7) Gao, M.-R.; Xu, Y.-F.; Jiang, J.; Yu, S.-H. Nanostructured Metal Chalcogenides: Synthesis, Modification, and Applications in Energy Conversion and Storage Devices. *Chem. Soc. Rev.* **2013**, *42* (7), 2986−3017.
(8) Pumera, M.; Sofer, Z.; Ambrosi, A. Layered Transition Metal Dichalcogenides for Electrochemical Energy Generation and Storage. *J. Mater. Chem. A* **2014**, *2*, 8981−8987.
(9) Jaramillo, T. F.; Jørgensen, K. P.; Bonde, J.; Nielsen, J. H.; Horch, S.; Chorkendorff, I. Identification of Active Edge Sites for Electrochemical H_2 Evolution from MoS_2 Nanocatalysts. *Science* **2007**, *317* (5834), 100−102.
(10) Ji, S.; Yang, Z.; Zhang, C.; Liu, Z.; Tjiu, W. W.; Phang, I. Y.; Zhang, Z.; Pan, J.; Liu, T. Exfoliated MoS_2 Nanosheets as Efficient Catalysts for Electrochemical Hydrogen Evolution. *Electrochim. Acta* **2013**, *109* (0), 269−275.

DOI: 10.1021/acsami.5b04672
ACS Appl. Mater. Interfaces 2015, 7, 17388−17398

(11) Lukowski, M. A.; Daniel, A. S.; Meng, F.; Forticaux, A.; Li, L.; Jin, S. Enhanced Hydrogen Evolution Catalysis from Chemically Exfoliated Metallic MoS_2 Nanosheets. *J. Am. Chem. Soc.* **2013**, *135* (28), 10274−10277.
(12) Wang, H.; Lu, Z.; Xu, S.; Kong, D.; Cha, J. J.; Zheng, G.; Hsu, P.-C.; Yan, K.; Bradshaw, D.; Prinz, F. B.; Cui, Y. Electrochemical Tuning of Vertically Aligned MoS_2 Nanofilms and Its Application in Improving Hydrogen Evolution Reaction. *Proc. Natl. Acad. Sci. U. S. A.* **2013**, *110* (49), 19701−19706.
(13) Stephenson, T.; Li, Z.; Olsen, B.; Mitlin, D. Lithium Ion Battery Applications of Molybdenum Disulfide (MoS_2) Nanocomposites. *Energy Environ. Sci.* **2014**, *7* (1), 209−231.
(14) David, L.; Bhandavat, R.; Singh, G. MoS_2/Graphene Composite Paper for Sodium-Ion Battery Electrodes. *ACS Nano* **2014**, *8* (2), 1759−1770.
(15) Novoselov, K. S.; Jiang, D.; Schedin, F.; Booth, T. J.; Khotkevich, V. V.; Morozov, S. V.; Geim, A. K. Two-Dimensional Atomic Crystals. *Proc. Natl. Acad. Sci. U. S. A.* **2005**, *102* (30), 10451−10453.
(16) Zhang, Y.; Zhang, L.; Zhou, C. Review of Chemical Vapor Deposition of Graphene and Related Applications. *Acc. Chem. Res.* **2013**, *46* (10), 2329−2339.
(17) Hernandez, Y.; Nicolosi, V.; Lotya, M.; Blighe, F. M.; Sun, Z.; De, S.; McGovern, I. T.; Holland, B.; Byrne, M.; Gun'Ko, Y. K.; Boland, J. J.; Niraj, P.; Duesberg, G.; Krishnamurthy, S.; Goodhue, R.; Hutchison, J.; Scardaci, V.; Ferrari, A. C.; Coleman, J. N. High-Yield Production of Graphene by Liquid-Phase Exfoliation of Graphite. *Nat. Nanotechnol.* **2008**, *3* (9), 563−568.
(18) Cunningham, G.; Lotya, M.; Cucinotta, C. S.; Sanvito, S.; Bergin, S. D.; Menzel, R.; Shaffer, M. S. P.; Coleman, J. N. Solvent Exfoliation of Transition Metal Dichalcogenides: Dispersibility of Exfoliated Nanosheets Varies Only Weakly between Compounds. *ACS Nano* **2012**, *6* (4), 3468−3480.
(19) Coleman, J. N.; Lotya, M.; O'Neill, A.; Bergin, S. D.; King, P. J.; Khan, U.; Young, K.; Gaucher, A.; De, S.; Smith, R. J.; Shvets, I. V.; Arora, S. K.; Stanton, G.; Kim, H.-Y.; Lee, K.; Kim, G. T.; Duesberg, G. S.; Hallam, T.; Boland, J. J.; Wang, J. J.; Donegan, J. F.; Grunlan, J. C.; Moriarty, G.; Shmeliov, A.; Nicholls, R. J.; Perkins, J. M.; Grieveson, E. M.; Theuwissen, K.; McComb, D. W.; Nellist, P. D.; Nicolosi, V. Two-Dimensional Nanosheets Produced by Liquid Exfoliation of Layered Materials. *Science* **2011**, *331* (6017), 568−571.
(20) Simon, P.; Gogotsi, Y. Materials for Electrochemical Capacitors. *Nat. Mater.* **2008**, *7* (11), 845−854.
(21) Conway, B. E.; Birss, V.; Wojtowicz, J. The Role and Utilization of Pseudocapacitance for Energy Storage by Supercapacitors. *J. Power Sources* **1997**, *66* (1−2), 1−14.
(22) Augustyn, V.; Simon, P.; Dunn, B. Pseudocapacitive Oxide Materials for High-Rate Electrochemical Energy Storage. *Energy Environ. Sci.* **2014**, *7* (5), 1597−1614.
(23) Conway, B. E.; Pell, W. G. Double-Layer and Pseudocapacitance Types of Electrochemical Capacitors and Their Applications to the Development of Hybrid Devices. *J. Solid State Electrochem.* **2003**, *7* (9), 637−644.
(24) Stoller, M. D.; Ruoff, R. S. Best Practice Methods for Determining an Electrode Material's Performance for Ultracapacitors. *Energy Environ. Sci.* **2010**, *3* (9), 1294−1301.
(25) Gogotsi, Y.; Simon, P. True Performance Metrics in Electrochemical Energy Storage. *Science* **2011**, *334* (6058), 917−918.
(26) Miller, J. R. Valuing Reversible Energy Storage. *Science* **2012**, *335* (6074), 1312−1313.
(27) Wu, S.; Zeng, Z.; He, Q.; Wang, Z.; Wang, S. J.; Du, Y.; Yin, Z.; Sun, X.; Chen, W.; Zhang, H. Electrochemically Reduced Single-Layer MoS_2 Nanosheets: Characterization, Properties, and Sensing Applications. *Small* **2012**, *8* (14), 2264−2270.
(28) Ambrosi, A.; Sofer, Z.; Pumera, M. Lithium Intercalation Compound Dramatically Influences the Electrochemical Properties of Exfoliated MoS_2. *Small* **2015**, *11* (5), 605−612.
(29) Acerce, M.; Voiry, D.; Chhowalla, M. Metallic 1T Phase MoS_2 Nanosheets as Supercapacitor Electrode Materials. *Nat. Nanotechnol.* **2015**, *10* (4), 313−318.
(30) Soon, J. M.; Loh, K. P. Electrochemical Double-Layer Capacitance of MoS_2 Nanowall Films. *Electrochem. Solid-State Lett.* **2007**, *10* (11), A250−A254.
(31) Cao, L.; Yang, S.; Gao, W.; Liu, Z.; Gong, Y.; Ma, L.; Shi, G.; Lei, S.; Zhang, Y.; Zhang, S.; Vajtai, R.; Ajayan, P. M. Direct Laser-Patterned Micro-Supercapacitors from Paintable MoS_2 Films. *Small* **2013**, *9* (17), 2905−2910.
(32) Lin, J.; Zhang, C.; Yan, Z.; Zhu, Y.; Peng, Z.; Hauge, R. H.; Natelson, D.; Tour, J. M. 3-Dimensional Graphene Carbon Nanotube Carpet-Based Microsupercapacitors with High Electrochemical Performance. *Nano Lett.* **2013**, *13* (1), 72−78.
(33) Beidaghi, M.; Wang, C. Micro-Supercapacitors Based on Interdigital Electrodes of Reduced Graphene Oxide and Carbon Nanotube Composites with Ultrahigh Power Handling Performance. *Adv. Funct. Mater.* **2012**, *22* (21), 4501−4510.
(34) El-Kady, M. F.; Strong, V.; Dubin, S.; Kaner, R. B. Laser Scribing of High-Performance and Flexible Graphene-Based Electrochemical Capacitors. *Science* **2012**, *335* (6074), 1326−1330.
(35) Winchester, A.; Ghosh, S.; Feng, S.; Elias, A. L.; Mallouk, T.; Terrones, M.; Talapatra, S. Electrochemical Characterization of Liquid Phase Exfoliated Two-Dimensional Layers of Molybdenum Disulfide. *ACS Appl. Mater. Interfaces* **2014**, *6* (3), 2125−2130.
(36) da Silveira Firmiano, E. G.; Rabelo, A. C.; Dalmaschio, C. J.; Pinheiro, A. N.; Pereira, E. C.; Schreiner, W. H.; Leite, E. R. Supercapacitor Electrodes Obtained by Directly Bonding 2D MoS_2 on Reduced Graphene Oxide. *Adv. Energy Mater.* **2014**, *4* (6), 1301380.
(37) Patil, S.; Harle, A.; Sathaye, S.; Patil, K. Development of a Novel Method to Grow Mono-/Few-Layered MoS_2 Films and MoS_2-Graphene Hybrid Films for Supercapacitor Applications. *CrystEngComm* **2014**, *16*, 10845−10855.
(38) Huang, K.-J.; Wang, L.; Liu, Y.-J.; Liu, Y.-M.; Wang, H.-B.; Gan, T.; Wang, L.-L. Layered MoS_2−Graphene Composites for Supercapacitor Applications with Enhanced Capacitive Performance. *Int. J. Hydrogen Energy* **2013**, *38* (32), 14027−14034.
(39) Feng, X.; Yan, Z.; Chen, N.; Zhang, Y.; Ma, Y.; Liu, X.; Fan, Q.; Wang, L.; Huang, W. The Synthesis of Shape-Controlled MnO_2/Graphene Composites *Via* a Facile One-Step Hydrothermal Method and Their Application in Supercapacitors. *J. Mater. Chem. A* **2013**, *1* (41), 12818−12825.
(40) Zhu, G.; He, Z.; Chen, J.; Zhao, J.; Feng, X.; Ma, Y.; Fan, Q.; Wang, L.; Huang, W. Highly Conductive Three-Dimensional MnO_2-Carbon Nanotube-Graphene-Ni Hybrid Foam as a Binder-Free Supercapacitor Electrode. *Nanoscale* **2014**, *6* (2), 1079−1085.
(41) Feng, X.; Chen, N.; Zhang, Y.; Yan, Z.; Liu, X.; Ma, Y.; Shen, Q.; Wang, L.; Huang, W. The Self-Assembly of Shape Controlled Functionalized Graphene-MnO_2 Composites for Application as Supercapacitors. *J. Mater. Chem. A* **2014**, *2* (24), 9178−9184.
(42) O'Neill, A.; Khan, U.; Coleman, J. N. Preparation of High Concentration Dispersions of Exfoliated MoS_2 with Increased Flake Size. *Chem. Mater.* **2012**, *24* (12), 2414−2421.
(43) Eda, G.; Yamaguchi, H.; Voiry, D.; Fujita, T.; Chen, M.; Chhowalla, M. Photoluminescence from Chemically Exfoliated MoS_2. *Nano Lett.* **2011**, *11* (12), 5111−5116.
(44) Lee, C.; Yan, H.; Brus, L. E.; Heinz, T. F.; Hone, J.; Ryu, S. Anomalous Lattice Vibrations of Single- and Few-Layer MoS_2. *ACS Nano* **2010**, *4* (5), 2695−2700.
(45) Li, H.; Zhang, Q.; Yap, C. C. R.; Tay, B. K.; Edwin, T. H. T.; Olivier, A.; Baillargeat, D. From Bulk to Monolayer MoS_2: Evolution of Raman Scattering. *Adv. Funct. Mater.* **2012**, *22* (7), 1385−1390.
(46) Benoist, L.; Gonbeau, D.; Pfister-Guillouzo, G.; Schmidt, E.; Meunier, G.; Levasseur, A. X-Ray Photoelectron Spectroscopy Characterization of Amorphous Molybdenum Oxysulfide Thin Films. *Thin Solid Films* **1995**, *258* (1−2), 110−114.
(47) Benoist, L.; Gonbeau, D.; Pfister-Guillouzo, G.; Schmidt, E.; Meunier, G.; Levasseur, A. XPS Analysis of Oxido-Reduction

DOI: 10.1021/acsami.5b04672
ACS Appl. Mater. Interfaces 2015, 7, 17388−17398

Mechanisms During Lithium Intercalation in Amorphous Molybdenum Oxysulfide Thin Films. *Solid State Ionics* **1995**, *76* (1−2), 81−89.
(48) Baker, M. A.; Gilmore, R.; Lenardi, C.; Gissler, W. XPS Investigation of Preferential Sputtering of S from MoS_2 and Determination of MoS_x Stoichiometry from Mo and S Peak Positions. *Appl. Surf. Sci.* **1999**, *150* (1−4), 255−262.
(49) Chang, Y.-H.; Lin, C.-T.; Chen, T.-Y.; Hsu, C.-L.; Lee, Y.-H.; Zhang, W.; Wei, K.-H.; Li, L.-J. Highly Efficient Electrocatalytic Hydrogen Production by MoS_x Grown on Graphene-Protected 3D Ni Foams. *Adv. Mater.* **2013**, *25* (5), 756−760.
(50) Demarconnay, L.; Raymundo-Piñero, E.; Béguin, F. A Symmetric Carbon/Carbon Supercapacitor Operating at 1.6 V by Using a Neutral Aqueous Solution. *Electrochem. Commun.* **2010**, *12* (10), 1275−1278.
(51) Huang, K.-J.; Wang, L.; Zhang, J.-Z.; Wang, L.-L.; Mo, Y.-P. One-Step Preparation of Layered Molybdenum Disulfide/Multi-Walled Carbon Nanotube Composites for Enhanced Performance Supercapacitor. *Energy* **2014**, *67*, 234−240.
(52) Ramadoss, A.; Kim, T.; Kim, G.-S.; Kim, S. J. Enhanced Activity of a Hydrothermally Synthesized Mesoporous MoS_2 Nanostructure for High Performance Supercapacitor Applications. *New J. Chem.* **2014**, *38* (6), 2379−2385.
(53) Conway, B. E. Transition from "Supercapacitor" to "Battery" Behavior in Electrochemical Energy Storage. *J. Electrochem. Soc.* **1991**, *138* (6), 1539−1548.
(54) Yang, L.; Cheng, S.; Ji, X.; Jiang, Y.; Zhou, J.; Liu, M. Investigations into the Origin of Pseudocapacitive Behavior of Mn_3O_4 Electrodes Using in Operando Raman Spectroscopy. *J. Mater. Chem. A* **2015**, *3*, 7338−7344.
(55) Brezesinski, T.; Wang, J.; Tolbert, S. H.; Dunn, B. Ordered Mesoporous α-MoO_3 with Iso-Oriented Nanocrystalline Walls for Thin-Film Pseudocapacitors. *Nat. Mater.* **2010**, *9* (2), 146−151.
(56) Liu, N.; Kim, P.; Kim, J. H.; Ye, J. H.; Kim, S.; Lee, C. J. Large-Area Atomically Thin MoS_2 Nanosheets Prepared Using Electrochemical Exfoliation. *ACS Nano* **2014**, *8* (7), 6902−6910.
(57) Zheng, J.; Zhang, H.; Dong, S.; Liu, Y.; Tai Nai, C.; Suk Shin, H.; Young Jeong, H.; Liu, B.; Ping Loh, K. High Yield Exfoliation of Two-Dimensional Chalcogenides Using Sodium Naphthalenide. *Nat. Commun.* **2014**, *5*, 2995.
(58) Béguin, F.; Presser, V.; Balducci, A.; Frackowiak, E. Carbons and Electrolytes for Advanced Supercapacitors. *Adv. Mater.* **2014**, *26* (14), 2219−2251.
(59) Cheng, Q.; Tang, J.; Ma, J.; Zhang, H.; Shinya, N.; Qin, L.-C. Graphene and Carbon Nanotube Composite Electrodes for Supercapacitors with Ultra-High Energy Density. *Phys. Chem. Chem. Phys.* **2011**, *13* (39), 17615−17624.
(60) Cheng, Q.; Tang, J.; Ma, J.; Zhang, H.; Shinya, N.; Qin, L.-C. Graphene and Nanostructured MnO_2 Composite Electrodes for Supercapacitors. *Carbon* **2011**, *49* (9), 2917−2925.
(61) Lewandowski, A.; Jakobczyk, P.; Galinski, M.; Biegun, M. Self-Discharge of Electrochemical Double Layer Capacitors. *Phys. Chem. Chem. Phys.* **2013**, *15* (22), 8692−8699.
(62) Conway, B. E.; Pell, W. G.; Liu, T. C. Diagnostic Analyses for Mechanisms of Self-Discharge of Electrochemical Capacitors and Batteries. *J. Power Sources* **1997**, *65* (1−2), 53−59.
(63) Oickle, A. M.; Andreas, H. A. Examination of Water Electrolysis and Oxygen Reduction as Self-Discharge Mechanisms for Carbon-Based, Aqueous Electrolyte Electrochemical Capacitors. *J. Phys. Chem. C* **2011**, *115* (10), 4283−4288.

DOI: 10.1021/acsami.5b04672
ACS Appl. Mater. Interfaces 2015, 7, 17388−17398